韓國電磁波學會論文誌 第 9 卷 第 2 號 1998年 4月 論文 98-9-2-03

Comparison with SAR Patterns of Biological Objects Contacted with Coaxial Waveguide Antenna Using MUR and GPML ABCs in the FDTD Method

유한차분법에서 MUR과 GPML 흡수경계조건을 이용한 동축 도파관 안테나에 접촉된 생체의 SAR 패턴 비교

Sung-Mo Koo* · Kwang-Hee Kwon · Chang-Won Lee · Chul-Ho Won · Jin-Ho Cho

구성모* · 권광희 · 이창원 · 원철호 · 조진호

요 약

동축 도파관 안테나에 접촉된 생체의 SAR 패턴을 계산하였고, 여기서 사용한 생체는 균질 및 4층 손실 인체 모델이다. 본 연구에서는 유한차분법 알고리즘과 MUR 및 GPML 흡수경계조건 방정식을 원통좌표계에서 유도하였다. 또한 매개체에서 흡수전력 패턴을 얻기 위하여 동축 도파관 안테나와 생체모델 사이의 결합을 유한차분법에서 MUR과 GPML 흡수경계조건을 사용하여 해석하였다. 온도분포와 일치하는 SAR 분포는 MUR 및 GPML 흡수경계조건을 사용한 유한차분법에서 정상상태 응답을 사용하여 각 영역에서 계산하였다. MUR 흡수경계조건을 사용한 유한차분법의 SAR 패턴을 GPML 흡수경계조건을 사용한 유한차분법의 SAR 패턴과 비교하였다. 비교 결과, MUR 흡수경계조건을 사용한 SAR 패턴의 침투 깊이가 GPML 흡수경계조건을 사용한 SAR 패턴의 침투 깊이보다 더 깊다는 것을 알 수 있었다. 이러한 현상은 GPML 흡수경계조건에서는 자유공간의 손실을 고려했기 때문이다. 그렇지만 GPML 흡수경계조건을 사용한 SAR 패턴의 측방향으로의 퍼짐이 MUR 흡수경계조건을 사용한 SAR 패턴보다 더 작다는 것을 알 수 있었다.

Abstract

The SAR patterns of biological objects contacted with coaxial waveguide antenna has been investigated, in which the biological object was modeled by a homogeneous and four-layered lossy human body. We derived the finite-difference time-domain(FDTD) algorithm and equation of MUR and generalized perfectly matched layer(GPML) ABCs in cylindrical coordination. The coupling between coaxial waveguide antenna and a biological object was analyzed by use of MUR and GPML ABCs in the FDTD method to obtain the absorbed power patterns in the media. The specific absorption rates (SAR) distribution which was corresponding to the temperature distribution was calculated in each region by use of the steady-state response in the FDTD method. The SAR patterns of the FDTD method using MUR absorbing boundary conditions(ABCs) was compared with those of the FDTD method

경북대학교 전자공학과(Department of Electronics, Kyungpook National University)
* 두원공업전문대학 전파통신과(Department of Radio Communication, Doowon Technical College)
· 논 문 번 호 : 971009-070
· 수정완료일자 : 1998년 2월 23일

using GPML ABCs. The comparison exhibits that the penetration depth of the SAR patterns using MUR ABCs is deeper than that of the SAR patterns using GPML ABCs because of loss in free space. However, the spread in the lateral directions of the SAR patterns using GPML ABCs is smaller than that of the SAR patterns using MUR ABCs.

I. Introduction

Typical tumors encountered in the clinic can range from 2 to 10 cm in diameter, and tumor sites vary from being on the skin surface to deep within the brain or pelvis. The primary objective of any hyperthermia system is to raise the temperature in the tumor volume to 43~55℃ while the surrounding normal tissue remains below 44℃.

Noninvasive microwave radiometry has been investigated for temperature measurement in human body. With currently available technique, invasive thermometers are used in the clinic. In this method, number and positions of thermometer probes that can be inserted in the patent's body are quite limited by trauma considerations, resulting often in inadequate thermometry. Inserting and locating the thermometer probes are laborious and time consuming tasks for doctors, besides the probe insertion gives discomfort to the patient. For these reasons, development of noninvasive technique of temperature measurement has been desired and studied for many years.

Recently, the waveguide antenna has been used in experimental investigations of multifrequency microwave radiometry to develop noninvasive techniques of constructing temperature profiles and map in biological objects [1],[2]. In these applications, the objects are lossy dielectric materials, such as a saline solution, phantom material, and a portion of human body. The portion of body coupled to the antenna is usually represented by a plane-parallel layered model consisting of, for example, the skin, fat and muscle. The problem of coupling between the rectangular waveguide antenna and the biological object of various configurations has been studied by a number of authors : Guy[3], Nikita[4], Mizoshiri[5] and Katsumi[6]. Rectangular waveguide as an excitation source was contacted with the different models of the biological object in these studies. It is difficult to contact practical biological object with the rectangular waveguide in the clinical applications because it is too hard to bend and heavy.

In this paper, a new type of the noninvasive hyperthermia technique which had not the above constraints was proposed and two models of human body were considered. One is the homogeneous model which is equivalent material with human muscle and the other is the four-layered model of human body. We derived the FDTD algorithm and equation of MUR and GPML ABCs in the cylindrical coordinates. The coupling between coaxial waveguide antenna and two model media was analyzed by use of MUR and GPML ABCs in the FDTD method to obtain the absorbed power pattern in the medium. The SAR distribution which was corresponding to the temperature distribution was calculated in each region by use of the steady-state response in

the FDTD method. The SAR patterns of the FDTD method using MUR ABCs was compared with those of the FDTD method using GPML ABCs. The comparison exhibits that the penetration depth of the SAR patterns using MUR ABCs is deeper than that of the SAR patterns using GPML ABCs because of loss in free space. However, the spread in the lateral directions of the SAR patterns using GPML ABCs is smaller than that of the SAR patterns using MUR ABCs.

Ⅱ. Description of the problem

The geometry of the problem is shown in Fig. 1, along the coordinate system, where a coaxial waveguide antenna with a finite flange is radiating into a four-layered lossy medium. The relative dielectric constant of the coaxial waveguide is $\varepsilon_r = 76.4$ and radii of inner and outer conductor(antenna) are a = 2.85 mm and b = 28.5 mm, respectively.

In our present study, we treat a homogeneous lossy medium and a four-layered lossy medium. The homogeneous medium is a 0.4% saline solution at 30 ℃ which is considered a muscle equivalent material. The four-layered medium is assumed to consist of distilled-water(14.25 mm), skin(1.9 mm), fat(14.25 mm) and muscle layer extending to infinity. Electrical properties of each material are listed in Table 1. Electrical properties of the saline solution and distilled-water(bolus) are obtained by Slogryan's equation[7], and those of the skin, fat and muscle are taken from Johnson and Guy[8].

The fundamental TEM mode is given at a plane normal to the waveguide axis which is 0.6λ away from coaxial end point as a source, as shown in Fig. 1, where λ is the wavelength in the coaxial waveguide. The incident electric field(source) E_ρ at the reference plane is given by

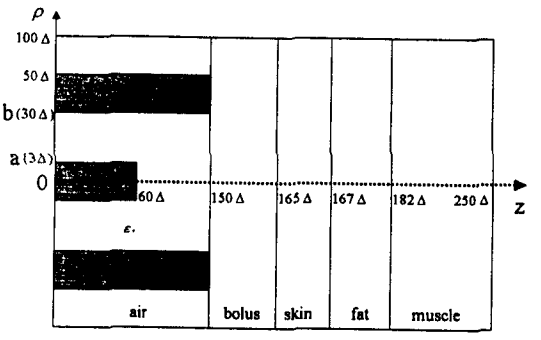

Fig. 1. Geometry of a coaxial antenna with a finite flange in contact with a four layered object.

$$E_\rho^i(\rho, t) = \frac{\sin \omega t}{\ln(\frac{b}{a})\rho}, \quad (1)$$

where ω is the angular frequency.

Table 1. Electrical properties of biological materials used in this paper.

	Dielectric constant(ε)	Conductivity (σ : S/m)
0.4% saline solution(30 ℃)	75.1	1.0
Skin	49.7	1.7
Fat	5.6	0.16
Muscle	49.7	1.7
Bolus (distilled-water)	76.4	0.26

In this paper, operating frequency is 1.2 GHz. The FDTD method is used to calculate electromagnetic field in each region. Size of the cubic Yee cell is taken as $\triangle = 0.95$ mm $\approx \lambda/30$.

Ⅲ. Yee's Algorithm

Yee[9] expressed Maxwell's curl equations in their finite-difference form. The Maxwell's curl equations used in the Yee/FDTD algorithm are

$$\nabla \times H = \frac{\partial D}{\partial t} + J, \quad \nabla \times E = -\frac{\partial B}{\partial t} \tag{2}$$

By expressing a continuous function of space and time in its discretized form, a function at its(nth) time step can be rewritten as

$$F^n(i, k) = F(i\triangle\rho, k\triangle z, n\triangle t) \tag{3}$$

After approximating the differential equations as difference equations and simplifying, following equations were obtained[10]

3-1 FDTD algorithm in MUR boundary

$$H_\Phi^{n+0.5}(i, k) = H_\Phi^{n-0.5}(i, k) + \frac{\triangle t}{\mu_0 \triangle \rho} [E_z^n(i+0.5, k) - E_z^n(i-0.5, k)] - \frac{\triangle t}{\mu_0 \triangle z} [E_\rho^n(i, k+0.5) - E_\rho^n(i, k-0.5)] \tag{4a}$$

$$E_\rho^{n+1}(i, k-0.5) = \frac{1 - \dfrac{\sigma(i, k-0.5)}{2\varepsilon(i, k-0.5)}}{1 + \dfrac{\sigma(i, k-0.5)}{2\varepsilon(i, k-0.5)}} E_\rho^n(i, k-0.5) - \frac{\dfrac{\triangle t}{\varepsilon(i, k-0.5)\triangle z}}{1 + \dfrac{\sigma(i, k-0.5)}{2\varepsilon(i, k-0.5)}} [H_\Phi^{n+0.5}(i, k) - H_\Phi^{n+0.5}(i, k-1)] \tag{4b}$$

$$E_z^{n+1}(i+0.5, k) = \frac{1 - \dfrac{\sigma(i+0.5, k)}{2\varepsilon(i+0.5, k)}}{1 + \dfrac{\sigma(i+0.5, k)}{2\varepsilon(i+0.5, k)}} E_z^n(i+0.5, k) - \frac{\dfrac{\triangle t}{\varepsilon(i+0.5, k)\,\rho(i+0.5, k)\triangle \rho}}{1 + \dfrac{\sigma(i+0.5, k)}{2\varepsilon(i+0.5, k)}} [\rho(i+1, k) H_\Phi^{n+0.5}(i+1, k) - \rho(i, k) H_\Phi^{n+0.5}(i, k)] \tag{4c}$$

where $\triangle\rho$ and $\triangle z$ are the space increments in ρ and z directions, respectively. $\triangle t$ is time increment, c is the light velocity, σ is conductivity, ε is dielectric constant, μ_0 is permeability in free space and meet the stability criteria as set forth by Taflove[9] and given by

$$\triangle t \le \frac{1}{c} \sqrt{\frac{1}{\dfrac{1}{\triangle \rho^2} + \dfrac{1}{\triangle z^2}}} \tag{5}$$

3-2 FDTD algorithm in GPML layer

$$H_\Phi^{n+0.5}(i, k) = H_\Phi^{n-0.5}(i, k) + \frac{\triangle t}{\mu \triangle \rho} [E_z^n(i+0.5, k) - E_z^n(i-0.5, k)] - \frac{\triangle t}{\mu \triangle z} [E_\rho^n(i, k+0.5) - E_\rho^n(i, k-0.5)] \tag{6a}$$

$$E_\rho^{n+1}(i, k-0.5) = \frac{2\varepsilon(i, k-0.5) - [\sigma_m(i, k-0.5) + \sigma_{gpml}(i, k-0.5)]\triangle t}{2\varepsilon(i, k-0.5) + [\sigma_m(i, k-0.5) + \sigma_{gpml}(i, k-0.5)]\triangle t} E_\rho^n(i, k-0.5)$$

$$-\frac{2\sigma_m(i,\,k-0.5)\sigma_{gpml}(i,\,k-0.5)(\triangle t)^2}{2\varepsilon^2(i,\,k-0.5)+\sigma(i,\,k-0.5)[\sigma_m(i,\,k-0.5)+\sigma_{gpml}(i,\,k-0.5)]\triangle t}$$

$$\sum_{p=0}^{n} E_\rho^p(i,\,k-0.5)-\frac{1}{s(i,\,k)\triangle z}$$

$$\frac{2\triangle t}{2\varepsilon(i,\,k-0.5)+[\sigma_m(i,\,k-0.5)+\sigma_{gpml}(i,\,k-0.5)]\triangle t}$$

$$[H_\Phi^{n+0.5}(i,\,k)-H_\Phi^{n+0.5}(i,\,k-1)] \qquad (6b)$$

$$E_z^{n+1}(i-0.5,\,k)=$$

$$\frac{2\varepsilon(i-0.5,\,k)-[\sigma_m(i-0.5,\,k)+\sigma_{gpml}(i-0.5,\,k)]\triangle t}{2\varepsilon(i-0.5,\,k)+[\sigma_m(i-0.5,\,k)+\sigma_{gpml}(i-0.5,\,k)]\triangle t}E_z^n(i-0.5,\,k)$$

$$-\frac{2\sigma_m(i-0.5,\,k)\sigma_{gpml}(i-0.5,\,k)(\triangle t)^2}{2\varepsilon^2(i-0.5,\,k)+\sigma(i-0.5,\,k)[\sigma_m(i-0.5,\,k)+\sigma_{gpml}(i-0.5,\,k)]\triangle t}$$

$$\sum_{p=0}^{n} E_z^p(i-0.5,\,k)-\frac{1}{s(i,\,k)\rho(i-0.5,\,k)\triangle\rho}$$

$$\frac{2\triangle t}{2\varepsilon(i-0.5,\,k)+[\sigma_m(i-0.5,\,k)+\sigma_{gpml}(i-0.5,\,k)]\triangle t}$$

$$\times[\rho(i,\,k)H_\Phi^{n+0.5}(i,\,k)-\rho(i-1,\,k)H_\Phi^{n+0.5}(i-1,\,k)] \qquad (6c)$$

where $\triangle\rho$ and $\triangle z$ are the space increments in ρ and z directions, respectively. $\triangle t$ is time increment, c is the light velocity, $s(i,\,k)$ is a coefficient, which serves to increase both real and imaginary parts of wave impedance. σ_m is electric conductivity in the medium, and σ_{gpml} is electric conductivity in GPML region.

Ⅳ. Absorbing boundary conditions

In order to model infinite space, boundary conditions at the computational lattice boundaries are needed. Since the computational lattice cannot be infinite for practical calculation, a finite region is used to model infinite space. When calculations stop at a fixed point in space, reflections occur at these computational boundaries. Lattice truncation conditions at the computation boundaries which simulate those of infinite space are therefore required. These absorbing boundary conditions absorb fields that are incident on the boundaries such that reflections do not occur. In our computation, the second-order absorbing boundary conditions based on MUR ABCs[11] and GPML ABCs[13],[14] in the cylindrical coordinates are used on the truncation boundaries. The magnetic fields on the upper and left peripheries of the truncation boundary in Fig. 1 are given by the following equation,

4-1 MUR ABCs

$$H_\Phi^{n+1}(N_{ie},\,k)=-\frac{\rho(N_{ie},\,k)}{\rho(N_{ie}-1,\,k)}$$

$$\frac{4c\triangle t\,\rho(N_{ie}-1,\,k)-c\triangle t\triangle\rho+4\triangle\rho\,\rho(N_{ie}-1,\,k)}{4c\triangle t\,\rho(N_{ie},\,k)+c\triangle t\triangle\rho+4\triangle\rho\,\rho(N_{ie},\,k)}$$

$$H_\Phi^{n-1}(N_{ie}-1,\,k)+\frac{\rho(N_{ie},\,k)}{\rho(N_{ie}-1,\,k)}$$

$$\frac{4c\triangle t\,\rho(N_{ie}-1,\,k)-c\triangle t\triangle\rho+4\triangle\rho\,\rho(N_{ie}-1,\,k)}{4c\triangle t\,\rho(N_{ie},\,k)+c\triangle t\triangle\rho+4\triangle\rho\,\rho(N_{ie},\,k)}$$

$$H_\Phi^{n+1}(N_{ie}-1,\,k)+\frac{4c\triangle t\,\rho(N_{ie},\,k)+c\triangle t\triangle\rho-4\triangle\rho\,\rho(N_{ie},\,k)}{4c\triangle t\,\rho(N_{ie},\,k)+c\triangle t\triangle\rho+4\triangle\rho\,\rho(N_{ie},\,k)}$$

$$H_\Phi^{n-1}(N_{ie},\,k)+\frac{8\triangle\rho\,\rho(N_{ie},\,k)}{4c\triangle t\,\rho(N_{ie},\,k)+c\triangle t\triangle\rho+4\triangle\rho\,\rho(N_{ie},\,k)}$$

$$[H_\Phi^n(N_{ie},\,k)+H_\Phi^n(N_{ie}-1,\,k)]+\frac{1}{(\triangle z)^2}$$

$$\frac{2(c\triangle t)^2\,\triangle\rho\,\rho(N_{ie},\,k)}{4c\triangle t\,\rho(N_{ie},\,k)+c\triangle t\triangle\rho+4\triangle\rho\,\rho(N_{ie},\,k)}[H_\Phi^n(N_{ie},\,k+1)$$

$$-2H_\Phi^n(N_{ie},\,k)+H_\Phi^n(N_{ie},\,k-1)+H_\Phi^n(N_{ie}-1,\,k+1)$$

$$-2H_\Phi^n(N_{ie}-1,\,k)+H_\Phi^n(N_{ie}-1,\,k-1)]$$

$$+\frac{1}{2}\,\frac{(c\triangle t)^2\,\triangle\rho\,\rho(N_{ie},\,k)}{4c\triangle t\,\rho(N_{ie},\,k)+c\triangle t\triangle\rho+4\triangle\rho\,\rho(N_{ie},\,k)}$$

$$\left[\frac{H_\Phi^n(N_{ie},\,k)}{\rho^2(N_{ie},\,k)}+\frac{H_\Phi^n(N_{ie}-1,\,k)}{\rho^2(N_{ie}-1,\,k)}\right] \qquad (7a)$$

$$H_\Phi^{n+1}(i,\,0)=-H_\Phi^{n-1}(i,\,1)$$

$$+\frac{c\triangle t-\triangle z}{c\triangle t+\triangle z}[H_{\Phi}^{n-1}(i,0)+H_{\Phi}^{n+1}(i,1)]$$
$$+\frac{2\triangle z}{c\triangle t+\triangle z}[H_{\Phi}^{n}(i,0)+H_{\Phi}^{n}(i,1)]$$
$$+\frac{(c\triangle t)^2\triangle z}{2(\triangle\rho)^2(c\triangle t+\triangle z)}[H_{\Phi}^{n}(i+1,0)-2H_{\Phi}^{n}(i,0)$$
$$+H_{\Phi}^{n}(i-1,0)+H_{\Phi}^{n}(i+1,1)-2H_{\Phi}^{n}(i,1)+H_{\Phi}^{n}(i-1,1)]$$
$$+\frac{(c\triangle t)^2\triangle z}{4(\triangle\rho)\rho_i\,(c\triangle t+\triangle z)}[H_{\Phi}^{n}(i+1,0)-H_{\Phi}^{n}(i-1,0)$$
$$+H_{\Phi}^{n}(i+1,1)-H_{\Phi}^{n}(i-1,1)] \quad [7b]$$

where N_{ie} is the truncation number in ρ-direction.

4-2 GPML ABCs

$$H_{\Phi\rho}^{n+0.5}(i,k)=\frac{2\mu-\sigma^*_{gpml}(i,k)\triangle t}{2\mu+\sigma^*_{gpml}(i,k)\triangle t}H_{\Phi\rho}^{n-0.5}(i,k)$$
$$-\frac{2\triangle t}{s(i,k)[2\mu+\sigma^*_{gpml}(i,k)\triangle t]\triangle z}$$
$$[E_{\rho}^{n}(i,k+0.5)-E_{\rho}^{n}(i,k-0.5)] \quad (8a)$$

$$H_{\Phi z}^{n+0.5}(i,k)=\frac{2\mu-\sigma^*_{gpml}(i,k)\triangle t}{2\mu+\sigma^*_{gpml}(i,k)\triangle t}H_{\Phi z}^{n-0.5}(i,k)$$
$$-\frac{2\triangle t}{s(i,k)[2\mu+\sigma^*_{gpml}(i,k)\triangle t]\triangle\rho}$$
$$[E_{z}^{n}(i+0.5,k)-E_{z}^{n}(i-0.5,k)] \quad (8b)$$

$$s(x)=1+s_m\left(\frac{x}{\delta}\right)^2 \quad (8c)$$

$$\sigma_{gpml}(x)=\sin^2\left(\frac{\pi x}{2\delta}\right)^2 \quad (8d)$$

where σ^*_{gpml} is magnetic conductivity in the GPML region, μ is permeability, $s(i,k)$ and s_m are coefficients, and δ is the absorber thickness.

V. Simulation results

In this section, results of the FDTD computation at 1.2 GHz operating frequencies are presented for two distinct cases:

(1) the antenna with the finite flange radiating into the homogeneous lossy medium,

(2) the antenna with the finite flange radiating into the four-layered medium.

The computation results are presented in the form of the SAR distribution[12] that in given by following equation.

$$SAR(i,k)=\frac{1}{2}\times\sigma(i,k)$$
$$\times[E_{\rho}^{2}(i,k)+E_{z}^{2}(i,k)] \quad (9)$$

where E_ρ and E_z are computed from the positive and negative peak values in the FDTD analysis. The SAR is proportional to temperature increment because it is energy absorption rates. Fig. 2 shows the SAR distribution using MUR and GPML ABCs in the homogeneous lossy medium.

Fig. 3 shows the SAR distribution using MUR and GPML ABCs in the four-layered medium. The pattern indicates that the SAR distributions spread out in the lateral directions, and the spreading is much larger than in the homogeneous medium. As consequence of the lateral spreading of the radiated power, the distance of power penetration along the z-axis is smaller in the four layered medium (using MUR ABCs : z=4.9 cm, using GPML ABCs: z=4.6 cm in Fig. 3) than in the homogeneous medium(using MUR ABCs: z=7.5 cm, using GPML ABCs: z=6.5 cm in Fig. 2).

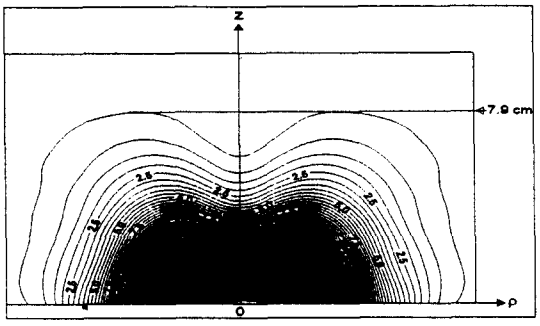

(a) using MUR ABCs

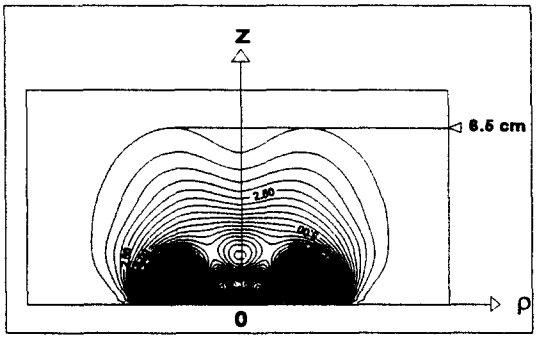

(b) using GPML ABCs

Fig. 2. SAR distribution in the homogeneous lossy medium for the antenna with the finite flange.

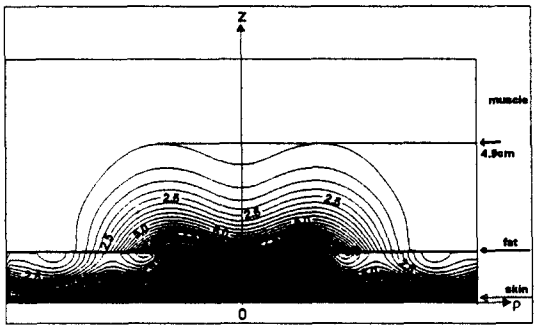

(a) using MUR ABCs

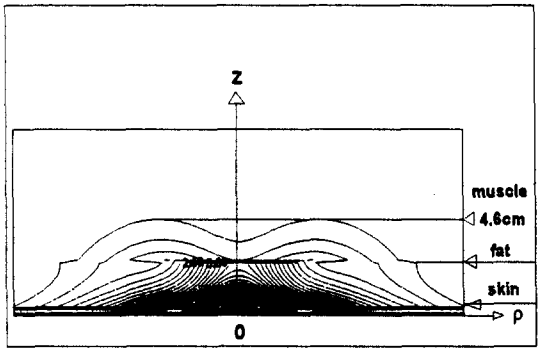

(b) using GPML ABCs

Fig. 3. SAR distribution in the four-layered medium for the antenna with the finite flange.

The SAR distribution in the four layered medium is affected very strongly by the presence of bolus and fat layers.

The lateral spreading of the electric fields in the four layered medium may be explained as following: a portion of the waves incident on the skin-fat and fat-muscle interfaces at oblique angles is reflected and trapped to excite waves propagating out in the lateral directions in the bolus and fat layer, and consequently in the skin layer as well. This phenomenon becomes stronger due to stronger diffraction by the antenna at lower operating frequencies.

The SAR patterns of the FDTD method using MUR ABCs was compared with those of the FDTD method using GPML ABCs. The comparison exhibits that the penetration depth of the SAR patterns using MUR ABCs is deeper than that of the SAR patterns using GPML ABCs because of loss in free space. However, the spread in the lateral directions of the SAR patterns using GPML ABCs is smaller than that of the SAR patterns using MUR ABCs.

Ⅵ. Conclusion

The dielectric-filled coaxial waveguide antenna was designed for noninvasive hyperthermia application. We derived the FDTD algorithm and equation of MUR and GPML ABCs in the cylindrical coordinates. The coupling between a dielectric-filled coaxial waveguide antenna and a four-layered biological medium was analyzed by use of MUR and GPML ABCs in the FDTD method. The second order MUR and GPML ABCs in the cylindrical coordinates was used on the truncation boundaries to model infinite space. The SAR patterns were calculated to predict the penetration depth of the electromagnetic field(or the temperature distribution) in the four-layered and homogeneous models of the human body. The simulation results indicate that the SAR patterns tend to spread out in the lateral directions due to the presence of the bolus and the fat layer. The SAR patterns of the FDTD method using MUR ABCs was compared with those of the FDTD method using GPML ABCs. The comparison exhibits that the penetration depth of the SAR patterns using MUR ABCs is deeper than that of the SAR patterns using GPML ABCs because of loss in free space. However, the spread in the lateral directions of the SAR patterns using GPML ABCs is smaller than that of the SAR patterns using MUR ABCs. We are currently using the FDTD method to design a new type of coaxial waveguide antenna with proper flange dimensions to suppress the lateral spreading and to attain a deeper penetration depth of the SAR distribution.

참 고 문 헌

[1] S. Mizushina, T. Shimizu, K. Suzuki and T. Sugiura, "Retrival of Temperature-Depth Profiles in Biological Objects from Multifrequency Microwave Radiometric Data," *J. of Electromagnetic Wave and Appl.*, Special issue on short-range sensing, pp. 1515-1548, 1993.

[2] F. Bardati, V. J. Brown and P. Tognolatti, "Temperature Reconstructions in a Dielectric Cylinder by Multifrequency Microwave Radiometry," *J. of Electromagnetic Wave and Appl.*, Special issue on short-range sensing, pp. 1549-1571, 1993.

[3] A. W. Guy, "Electromagnetic Fields and Relative Heating Patterns Due to a Rectangular Aperture Source in Direct Contact with Bilayered Biological Tissue," *IEEE Trans. Microwave Theory & Tech.*, vol. MTT-19, pp. 214-223, 1971.

[4] K. S. Nikita and N. K. Uzunoglu, "Analysis of the Power Coupling from a Waveguide Hyperthermia Applicator into a Three-Layered Tissue Model," *IEEE Trans. Microwave Theory & Tech.*, vol. MTT-37, pp. 1794-1801, 1989.

[5] S. Mizoshiri, K. Abe, T. Sugiura and S. Mizushina, "Computation of the Field Distribution Generated by a Rectangular Aperture in Four-Layered Lossy Dielectric Medium by Modal Analysis," *IEICE Trans. Commun.*, vol. E78-B, no. 6, pp. 851-858, June 1995.

[6] K. Abe, S. Mizoshiri, T. Sugiura and S. Mizushina, "Electromagnetic Near Fields

of a Rectangular Waveguide Antenna in Contact with Biological Objects Obtained by the FDTD Method," *IEICE Trans. Commun.*, vol. E78-B, no. 6, pp. 866-870, June 1995.

[7] S. Slogryan, "Equations for Calculating the Dielectric Constant of Saline Water," *IEEE Trans. Microwave Theory & Tech.*, vol. MTT-19, pp. 733-736, 1971.

[8] C. C. Johnson and A. W. Guy, "Nonionizing Electromagnetic Wave Effects in Biological Materials and Systems," *Proc. IEEE*, vol. 60, pp. 692-718, 1972.

[9] A. Taflove and M. E. Brodwin, "Numerical Solution of Steady-State Electromagnetic Scattering Problems Using the Time Dependent Maxwell's Equations," *IEEE Trans. Microwave Theory & Tech.*, vol. MTT-23, pp. 623-630, 1975.

[10] A. Taflove, *Computational Electrodynamics : The Finite-Difference Time-Domain Method*, Artech House, Boston, 1995.

[11] G. Mur, "Absorbing Boundary Conditions for the Finite Difference Approximation of the Time-Domain Electromagnetic Field Equations," *IEEE Trans. Electromag. Compat.*, vol. EMC-23, pp. 377-382, 1981.

[12] D. Sullivan, "Three-Dimensional Computer Simulation in Deep Regional Hyperthermia Using the FDTD Method," *IEEE Trans. Microwave Theory & Tech.*, vol. MTT-38, pp. 204-211, 1990.

[13] J. Fang and Z. Wu, "Generalized Perfectly Matched Layer-An Extension of Berenger's Perfectly Matched Layer Boundary Condition," *IEEE Microwave and Guided Letters.*, vol. 5, pp. 451-453, 1995.

[14] Y. C. Lau, M. S. Leong and P. S. Kooi, "Extension of Berenger's PML Boundary Condition in Matching Lossy Medium and Evanescent Waves," *Electronics Letters.*, vol. 32, pp. 974-976, 1996.

구 성 모

1987년 2월 : 경북대학교 전자공학과(공학사)
1993년 2월 : 경북대학교 대학원 전자공학과(공학석사)
1993년 3월 ~ 현재 : 경북대학교 대학원 전자공학과(박사수료)
1995년 3월 ~ 현재 : 두원공업전문대학 전파통신과 조교수
[주 관심분야] 전자파 응용(생체), hyperthermia, 의용영상처리

권 광 희

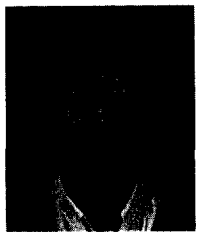

1995년 2월 : 경북대학교 전자공학과(공학사)
1997년 2월 : 경북대학교 대학원 전자공학과(공학석사)
1997년 3월 ~ 현재 : 경북대학교 대학원 전자공학과(박사과정)
[주 관심분야] 전자파 산란 및 안테나 해석

이 창 원

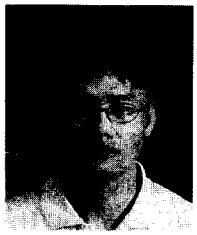

1991년 2월 : 경북대학교 전자공학과(공학사)

1993년 2월 : 경북대학교 대학원 전자공학과(공학석사)

1993년 3월 ~ 현재 : 경북대학교 대학원 전자공학과(박사수료)

[주 관심분야] 전자파 산란 및 안테나 해석

조 진 호

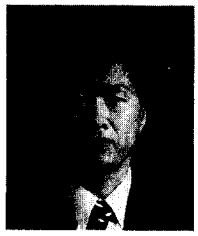

1977년 2월 : 경북대학교 공업교육과 전기전공(공학사)

1979년 2월 : 경북대학교 대학원 전자공학과(공학석사)

1988년 2월 : 경북대학교 대학원 전자공학과(공학박사)

1984년 ~ 현재 : 경북대학교 전자전기공학부 교수

1984년 ~ 현재 : 경북대학교 병원 의공실장 겸무

[주 관심분야] 의용신호처리, 센서의용계측, 센서응용 시스템 개발

원 철 호

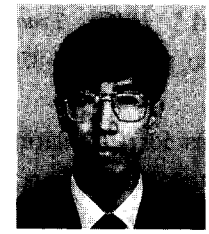

1992년 2월 : 경북대학교 전자공학과(공학사)

1995년 2월 : 경북대학교 대학원 전자공학과(공학석사)

1995년 3월 ~ 현재 : 경북대학교 대학원 전자공학과(박사수료)

1998년 3월~현재 : 계명대학교 동산의료원 의공학과 연구강사

[주 관심분야] 의학영상처리, 의용신호처리, 디지털하드웨어